ELSEVIER

Journal of Alloys and Compounds 461 (2008) 117–120

Journal of ALLOYS AND COMPOUNDS

www.elsevier.com/locate/jallcom

Origin of three-stage transformation in a severely cold-rolled and annealed $Ti_{51}Ni_{40}Cu_9$ shape memory alloy

K.N. Lin [a], S.K. Wu [a,b,*]

[a] *Department of Materials Science and Engineering, National Taiwan University, Taipei 106, Taiwan*
[b] *Department of Mechanical Engineering, National Taiwan University, Taipei 106, Taiwan*

Received 29 May 2007; received in revised form 4 July 2007; accepted 4 July 2007
Available online 10 July 2007

Abstract

Severely cold-rolled $Ti_{51}Ni_{40}Cu_9$ shape memory alloy annealed at 500 °C × 72 h and 650 °C × 1 h exhibits three-stage martensitic transformation owing to the grain-size effect, i.e., the specimen has small grains near the rolling surfaces and large grains in the central region. The different grain-size distribution is attributed to the inhomogeneous cold-rolling effect. The three-stage transformation has three pairs of transformation peaks which are associated with $B2_1 \leftrightarrow B19_1$ transformation of large grains, $B2_2 \leftrightarrow B19_2$ transformation of small grains and $(B19_1 + B19_2) \leftrightarrow B19'$ transformation of both large and small grains.

Keywords: Metals and alloys; Shape memory; Phase transformation; Thermal analysis

1. Introduction

TiNi-based shape memory alloys (SMAs) have great potential for mechanical, biomedical and sports applications because of their excellent properties on shape memory effect (SME), pseudoelasticity (PE) and damping capacity [1]. The substitution of Cu for Ni in TiNi SMAs has been known to reduce or prevent the following events: (1) the composition sensitivity of the starting temperature for martensitic transformation, M_s [2], (2) the hysteresis of pseudoelasticity [3], and (3) the flow stress level in the martensitic state [3,4]. $Ti_{50}Ni_{50-x}Cu_x$ SMAs, with $x < 30$ at.%, have been investigated extensively from various aspects. Transformation sequences of $Ti_{50}Ni_{50-x}Cu_x$ SMAs are $B2 \leftrightarrow B19'$, $B2 \leftrightarrow B19 \leftrightarrow B19'$ and $B2 \leftrightarrow B19$ for $x < 5$, $5 < x < 20$ and $x > 20$ at.%, respectively [5–7]. Here B2 is parent austenite, B19 and B19′ are orthorhombic and monoclinic martensite, respectively.

Multi-stage martensitic transformation is usually found in aged Ni-rich TiNi SMAs [8–13]. All the complex multi-stage martensitic transformations appeared in Ni-rich TiNi alloys are associated with the heterogeneous stress field caused by Ti_3Ni_4 precipitates and the inhomogeneous distribution of Ti_3Ni_4 precipitates. We have recently reported the occurrence of the multi-stage martensitic transformations owing to different grain-size distribution in cold-rolled and annealed bulk $Ti_{50}Ni_{50}$ SMA [14] and in annealed melt-spun $Ti_{51}Ni_{49}$ SMA ribbons [15]. In the present study, a three-stage martensitic transformation is found in a cold-rolled and annealed $Ti_{51}Ni_{40}Cu_9$ SMA. The transformation characteristics of this three-stage martensitic transformation are systematically investigated by differential scanning calorimetry (DSC), dynamic mechanical analyzer (DMA) and optical microscope (OM). The cause of this three-stage martensitic transformation is also discussed.

2. Experimental procedure

$Ti_{51}Ni_{40}Cu_9$ ingot was prepared by conventional vacuum arc-remelting (VAR) method in which high-purity Ti (99.8 wt.%), Ni (99.9 wt.%) and Cu (99.99 wt.%) were remelted six times in a high-purity Ar atmosphere. The as-melted ingot was hot-rolled at 900 °C to a plate of about 2.0 mm thickness by STANAT TA-515-5-5X8 rolling machine at a constant rolling speed of 10 m/min, then solution-treated at 900 °C for 1 h and subsequently quenched in water. The oxidation layer of the plate was chemically etched by a solution composed of $HF:HNO_3:H_2O = 1:5:20$ (v/v/v) and then polished by #150 sandpapers. After removing the oxidation layer, the plate became about 1.8 mm in thickness, and was cut into 75 mm × 20 mm strips with the longitude along the hot-rolling direction. Thereafter, the strips were cold-rolled to 1 mm in thickness at room

* Corresponding author at: Department of Materials Science and Engineering, National Taiwan University, Taipei 106, Taiwan. Tel.: +886 2 2363 7846; fax: +886 2 2363 4562.
E-mail address: skw@ntu.edu.tw (S.K. Wu).

0925-8388/$ – see front matter © 2007 Elsevier B.V. All rights reserved.
doi:10.1016/j.jallcom.2007.07.010

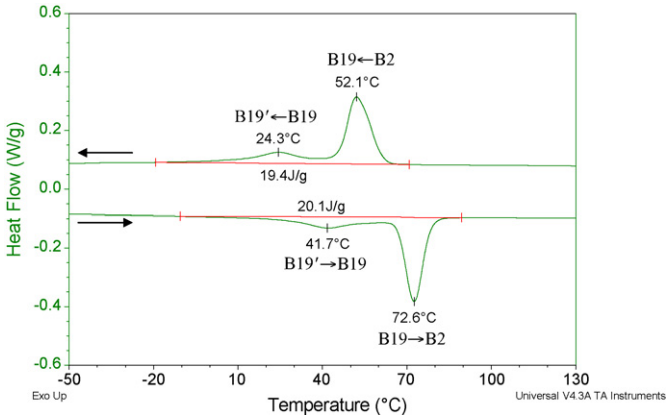

Fig. 1. DSC result of as hot-rolled $Ti_{51}Ni_{40}Cu_9$ specimen.

temperature along the hot-rolling direction by the same rolling machine with about 2% thickness reduction for each pass. The total reduction in thickness was about 44%. After cold-rolling, the strips were cut into 35 mm × 4.5 mm × 1 mm specimens for DMA test and about 30 mg specimens for DSC test, sealed in evacuated quartz tubes and then annealed in 500 °C and 650 °C salt baths for different time intervals.

Transformation temperature and enthalpy of cold-rolled and annealed $Ti_{51}Ni_{40}Cu_9$ specimens were determined by TA Q10 DSC equipment at 10 °C/min cooling/heating rate. Their internal friction (tan δ) values were determined by TA 2980 DMA equipment at 3 °C/min cooling rate under 1 Hz frequency and 5 μm amplitude. The testing temperature ranged from +150 °C to −120 °C in both DSC and DMA tests. The cross-sectional microstructure of cold-rolled and annealed $Ti_{51}Ni_{40}Cu_9$ specimens was observed by Nikon FX-35DX optical microscope (OM). The electro-polish was done under 5 V at room temperature. The electro-polishing solution was composed of $CH_3COOH:HClO_4 = 5:95$ (v/v). From the OM images, the average grain size of cold-rolled and annealed specimens was estimated by the linear intercept method [16].

3. Results and discussion

3.1. DSC and DMA results of as hot-rolled $Ti_{51}Ni_{40}Cu_9$ specimen

Figs. 1 and 2 show DSC and DMA results of as hot-rolled $Ti_{51}Ni_{40}Cu_9$ specimen, respectively. In Figs. 1 and 2, as hot-rolled $Ti_{51}Ni_{40}Cu_9$ specimen shows a two-stage transformation corresponding to two exothermal peaks, two tan δ peaks and two storage modulus minima during cooling. According to our previous study [17], the first transformation is B2 → B19, corresponds to a sharp exothermal peak, a sharp tan δ peak and a significant storage modulus drop; while the second transformation is B19 → B19′, corresponds to a broad exothermal peak, a broad tan δ peak and a minute storage modulus drop. Thus the transformation sequence of $Ti_{51}Ni_{40}Cu_9$ specimen is the same as that of $Ti_{50}Ni_{50-x}Cu_x$ ($5 \le x \le 20$ at.%), i.e., B2 ↔ B19 ↔ B19′ two-stage transformation [5–7]. However, both B2 ↔ B19 and B19 ↔ B19′ transformation peak temperatures of $Ti_{51}Ni_{40}Cu_9$ specimen are higher than those of $Ti_{50}Ni_{40}Cu_{10}$ specimen [17] because the former has Ti-rich chemical composition. Moreover, there is a small temperature shift between the results of DSC and DMA tests which is attributed to the different cooling/heating rates and specimen sizes used in these two tests.

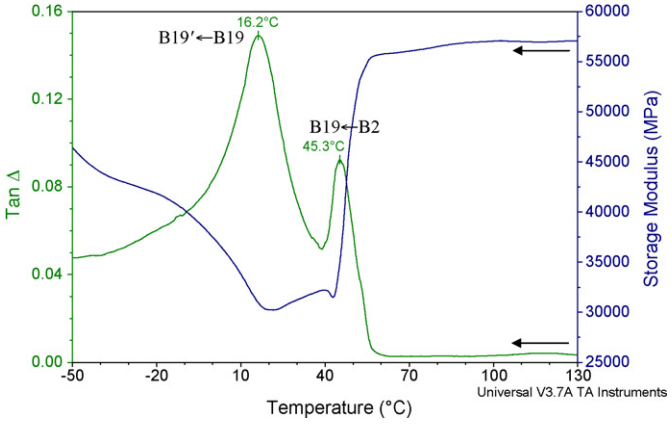

Fig. 2. DMA result of as hot-rolled $Ti_{51}Ni_{40}Cu_9$ specimen.

3.2. Cross-sectional microstructure of cold-rolled and annealed $Ti_{51}Ni_{40}Cu_9$ specimen

Fig. 3(a)–(c) show the OM micrographs of cross-sectional microstructure of cold-rolled $Ti_{51}Ni_{40}Cu_9$ specimen annealed at 650 °C × 1 h. Fig. 3(a) reveals that the microstructure in the central region is quite different from that near the specimen's rolling surfaces. The grains in the central region are elongated along the rolling direction (RD) and the average grain size is about 23 μm, as calculated from Fig. 3(b) and (c) shows that the

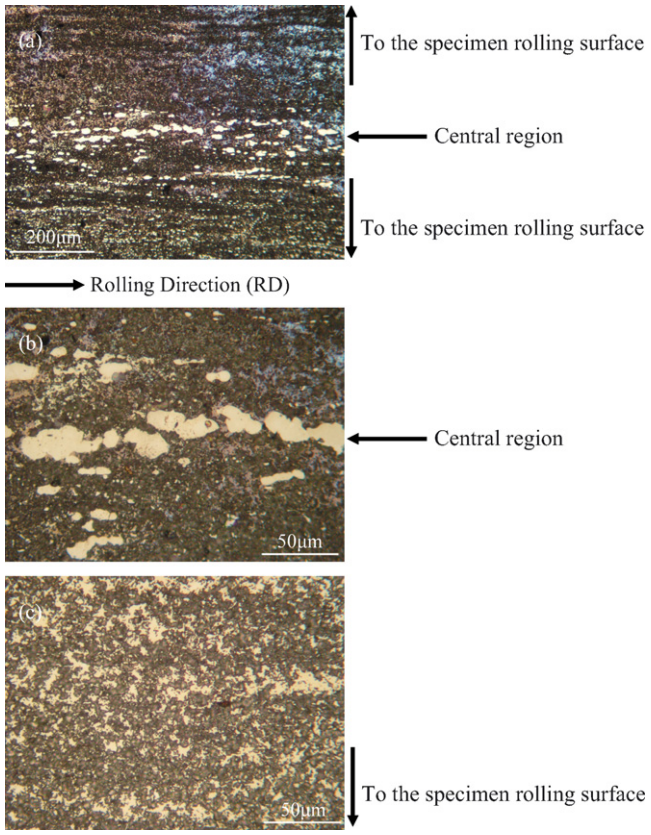

Fig. 3. OM micrographs of cross-sectional microstructure of cold-rolled $Ti_{51}Ni_{40}Cu_9$ specimen annealed at 650 °C × 1 h. (a) The full scope, (b) the enlarged central region and (c) the enlarged near rolling surface region.

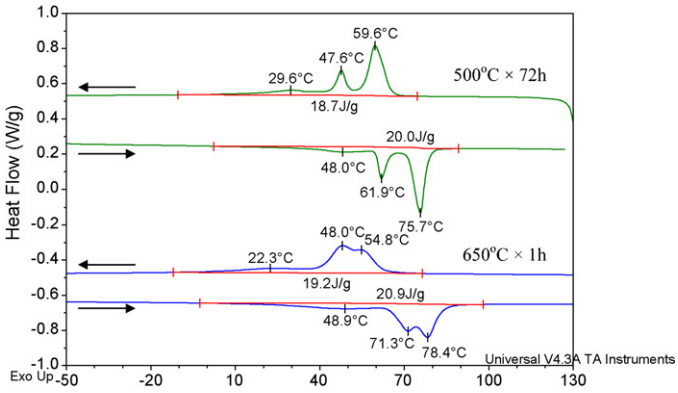

Fig. 4. DSC results of cold-rolled $Ti_{51}Ni_{40}Cu_9$ specimens annealed at 500 °C × 72 h and 650 °C × 1 h.

grains near the rolling surfaces are much finer than those in the central region and the grain size is about 3 μm. This is because the specimen's surfaces are in direct contact with the rollers and suffer more plastic deformation than the central region. The inhomogeneous microstructure shown in Fig. 3 is quite similar to that seen in our previous study for the 35% cold-rolled $Ti_{50}Ni_{50}$ SMA annealed at 500 °C × 3 h [14].

3.3. DSC results of cold-rolled and annealed $Ti_{51}Ni_{40}Cu_9$ specimen

Fig. 4 shows DSC results of cold-rolled $Ti_{51}Ni_{40}Cu_9$ specimens annealed at 500 °C × 72 h and 650 °C × 1 h. As can be seen, there are three transformation peaks in both cooling and heating curves. In order to identify these transformation peaks, the cooling process is interrupted at each transformation peak and immediately heats up to obtain the corresponding partial-cycle DSC curve. The partial-cycle results of the specimens annealed at 500 °C × 72 h are shown in Fig. 5. In Fig. 5, the solid line represents the full-cycle DSC curve, and the long-dash line represents the partial-cycle DSC curve which is interrupted at the first transformation peak, say 59.6 °C, and a reverse transformation peak appears at 75.7 °C during heating. Since the first pair of transformation peaks is quite sharp, we conclude that it is $B2_1 \leftrightarrow B19_1$ transformation associated with the central region

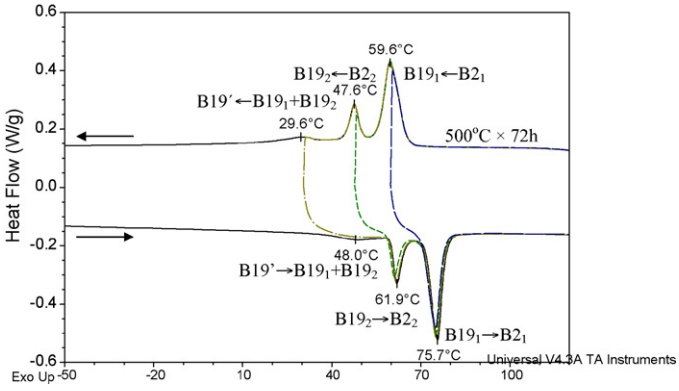

Fig. 5. The overlapped partial-cycle DSC results for cold-rolled $Ti_{51}Ni_{40}Cu_9$ specimen annealed at 500 °C × 72 h.

of the specimen which will be discussed in greater detail in the next section. In the same way, the short-dash line in Fig. 5 represents the partial-cycle DSC curve interrupted at the second transformation peak (47.6 °C), and a reverse transformation peak appears at 61.9 °C during heating. Since the second pair of transformation peaks is also quite sharp, we conclude that it is also $B2_2 \leftrightarrow B19_2$ transformation associated with the near-surface region of the specimen. Finally, the partial-cycle DSC test is interrupted at the third peak (≒29.6 °C and shown as the dash-dot line in Fig. 5), and a reverse transformation peak appears at 48.0 °C during heating. The last pair of transformation peaks is quite broad, and we conclude that it is $(B19_1 + B19_2) \leftrightarrow B19'$ transformation. All the transformations associated with these three pairs of transformation peaks are highlighted in Fig. 5.

The transformation sequence of cold-rolled $Ti_{51}Ni_{40}Cu_9$ specimen annealed at 650 °C × 1 h, as shown in Fig. 4, is the same as that of annealed at 500 °C × 72 h, i.e., the first, second and third pair of transformation peaks are associated with $B2_1 \leftrightarrow B19_1$, $B2_2 \leftrightarrow B19_2$ and $(B19_1 + B19_2) \leftrightarrow B19'$ transformations, respectively. However, the first and second pair of transformation peaks overlap partially.

3.4. Origin of three-stage martensitic transformation in cold-rolled and annealed $Ti_{51}Ni_{40}Cu_9$ specimen

In order to clarify the grain-size effect on three-stage martensitic transformation shown in Fig. 4, the cold-rolled and annealed $Ti_{51}Ni_{40}Cu_9$ specimens are ground from both rolling surfaces to remove the grains that are smaller than those in the central region. The thickness of the specimen annealed at 650 °C × 1 h is first reduced from 1 mm to 0.6 mm and then further reduced from 0.6 mm to 0.4 mm. Fig. 6(a) and (b) show the evolution of DSC curves corresponding to the specimen thickness. In Fig. 6, the second pair of $B2_2 \leftrightarrow B19_2$ peaks of the 0.6 mm-thick specimen becomes smaller than that of the 1.0 mm one. Moreover, for the 0.4 mm-thick specimen, $B2_2 \leftrightarrow B19_2$ peaks almost disappear. Also shown in Fig. 6, the transformation peak temperatures shift slightly to higher temperatures when the specimen's thickness is reduced. This is because the grinding process can eliminate the suppression effect of the abundant grain boundaries on the transformation temperature.

The specimen thickness of the $Ti_{51}Ni_{40}Cu_9$ specimen annealed at 500 °C × 72 h is also reduced from 1.0 mm to 0.4 mm. Fig. 7 shows the evolution of DMA cooling curves corresponding to the specimen thickness. For the DMA curve of the 0.4 mm-thick specimen, the $B2_2 \rightarrow B19_2$ peak almost disappears too.

The aforementioned DSC and DMA results of ground specimens suggest that the three-stage martensitic transformation shown in Fig. 4 comes from the grain-size effect. Here, $B2_1 \leftrightarrow B19_1$ is associated with B2 ↔ B19 transformation owing to the large grains in the central region, and $B2_2 \leftrightarrow B19_2$ is also associated with B2 ↔ B19 transformation, but attributed to the small grains near the rolling surfaces. The inhomogeneous cold-rolling deformation distributed in the specimen implies that the degree of plastic deformation in the central region is less than that near the rolling surfaces. As a result, the grains in the central

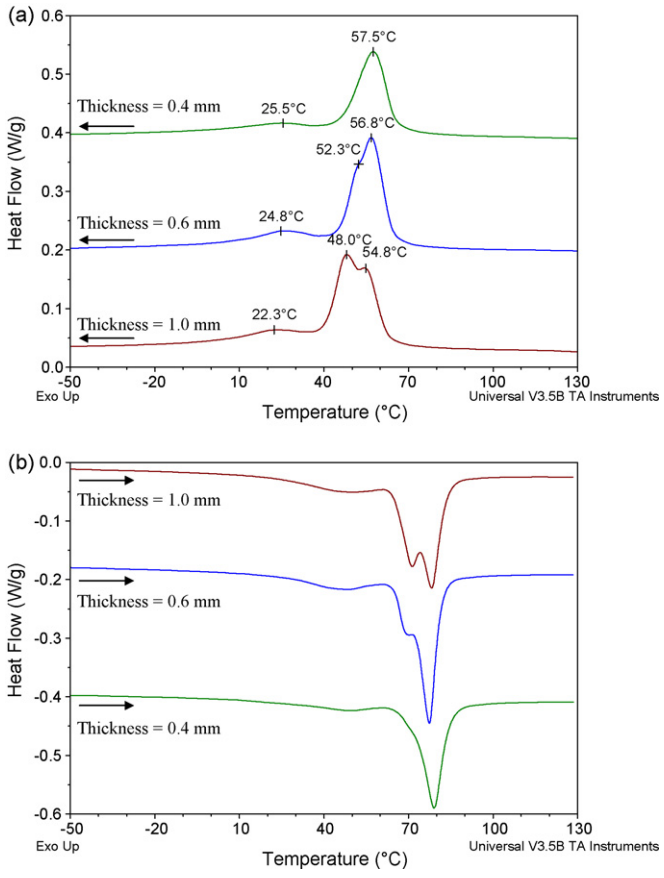

Fig. 6. DSC curves for cold-rolled $Ti_{51}Ni_{40}Cu_9$ specimen annealed at 650 °C × 1 h. (a) DSC cooling curves and (b) DSC heating curves.

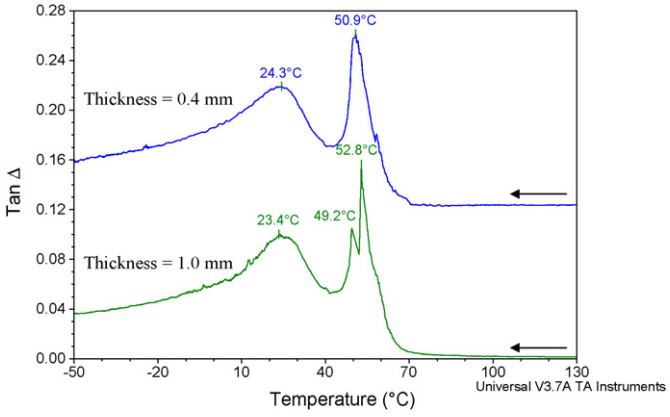

Fig. 7. DMA curves for cold-rolled $Ti_{51}Ni_{40}Cu_9$ specimen annealed at 500 °C × 72 h.

region are larger than those near the rolling surfaces after recrystallization and grain growth. It is well known that the defects such as grain boundaries can suppress martensitic transformation to a lower temperature [14]. Therefore, $B2_2 \leftrightarrow B19_2$ transformation corresponding to the smaller grains near the rolling surfaces takes place at lower temperature than $B2_1 \leftrightarrow B19_1$ transformation corresponding to the large grains in the central region.

Compared with $B2 \leftrightarrow B19$ transformation, $B19 \leftrightarrow B19'$ transformation shown in Fig. 4 does not separate into two $B19_1 \leftrightarrow B19_1'$ and $B19_2 \leftrightarrow B19_2'$ transformations which correspond to the large and small grains, respectively. This is because $B19 \leftrightarrow B19'$ transformation requires much smaller transformation strain (~2%) than $B2 \leftrightarrow B19$ transformation (~8%) [18]. Therefore, the effect of grain size can be neglected in $B19 \leftrightarrow B19'$ transformation.

4. Conclusions

The three-stage martensitic transformation occurring in severely cold-rolled $Ti_{51}Ni_{40}Cu_9$ SMA annealed at 500 °C × 72 h and 650 °C × 1 h is investigated by DSC, DMA and OM. Experimental results show that three-stage martensitic transformation is attributed to the different grain-size distribution, i.e., the small grains near the rolling surfaces and the large grains in the central region. Such distribution is attributed to the inhomogeneous cold-rolled effect in which the specimen's surfaces are in direct contact with the rollers and suffer more plastic deformation than the central region. The three-stage martensitic transformation has three pairs of transformation peaks which are associated with $B2_1 \leftrightarrow B19_1$ transformation of the large grains in the central region, $B2_2 \leftrightarrow B19_2$ transformation of the small grains near the rolling surfaces and $(B19_1 + B19_2) \leftrightarrow B19'$ transformation of both large and small grains.

Acknowledgement

The authors gratefully acknowledge the financial support from the National Science Council (NSC), Taiwan, Republic of China, under the Grant NSC95-2221-E002-164.

References

[1] C.M. Wayman, T.W. During, in: T.W. During, K.N. Melton, D. Stöckel, C.M. Wayman (Eds.), Engineering Aspects of Shape Memory Alloys, Butterworth-Heinemann, London, 1990, pp. 3–20.
[2] O. Mercier, K.N. Melton, Metall. Trans. 10A (1979) 387.
[3] T. Saburi, T. Takagaki, S. Nenno, K. Koshino, MRS Int. Manuf. Adv. Maters. 9 (1988) 147.
[4] J.L. Proft, K.N. Melton, T.W. Duerig, MRS Int. Manuf. Adv. Mats. 9 (1988) 159.
[5] H. Miyamato, T. Taniwaki, T. Ohba, K. Otsuka, S. Nishigori, K. Katc, Scripta Mater. 53 (2005) 171.
[6] T.H. Nam, T. Saburi, K. Shimizu, Mater. Trans., JIM 31 (1990) 959.
[7] T.H. Nam, T. Saburi, Y. Nakata, K. Shimizu, Mater. Trans., JIM 31 (1990) 1050.
[8] L. Bataillard, R. Gotthardt, J. Phys. III 5 (1995) C8–C647.
[9] L. Bataillard, J.-E. Bidaux, R. Gotthardt, Philos. Mag. 78 (1998) 327.
[10] J. Khalil-Allafi, A. Dlouhy, G. Eggeler, Acta Mater. 50 (2002) 4255.
[11] P.C. Su, S.K. Wu, Acta Mater. 52 (2004) 1117.
[12] J.I. Kim, Y. Liu, S. Miyazaki, Acta Mater. 52 (2004) 487.
[13] J. Michutta, Ch. Somsen, A. Yawny, A. Dlouhy, G. Eggeler, Acta Mater. 54 (2006) 3525.
[14] S.H. Chang, S.K. Wu, G.H. Chang, Scripta Mater. 52 (2005) 1341.
[15] K.N. Lin, S.K. Wu, J. Alloys Compd. 424 (2006) 171.
[16] ASTM Standards—Standards test method for determining average grain size. Annual book of ASTM standards, vol. 03.01.2003, p.256.
[17] Y.C. Lo, S.K. Wu, H.E. Horng, Acta Met. Mater. 41 (1993) 747.
[18] X. Ren, N. Miura, J. Zhang, K. Otsuka, K. Tanaka, M. Koiwa, T. Suzuki, Yu.I. Chumlyakov, M. Asai, Mater. Sci. Eng. A 312 (2001) 196.